

ESCAPE OF IONIZING RADIATION FROM HIGH REDSHIFT GALAXIES

NICKOLAY Y. GNEDIN^{1,2,3}, ANDREY V. KRAVTSOV^{2,3,4}, AND HSIAO-WEN CHEN³

Draft version February 1, 2008

ABSTRACT

We model the escape of ionizing radiation from high-redshift galaxies using high-resolution Adaptive Mesh Refinement N -body+hydrodynamics simulations. Our simulations include time-dependent and spatially-resolved transfer of ionizing radiation in three dimensions, including effects of dust absorption. For galaxies of total mass $M \gtrsim 10^{11} M_{\odot}$ and star formation rates $\text{SFR} \approx 1 - 5 M_{\odot} \text{ yr}^{-1}$, we find angular averaged escape fractions of 1–3% over the entire redshift interval studied ($3 < z < 9$). In addition, we find that the escape fraction varies by more than an order of magnitude along different lines-of-sight within individual galaxies, from the largest values near galactic poles to the smallest along the galactic disk. The escape fraction declines steeply at lower masses and SFR. We show that the low values of escape fractions are due to a small fraction of young stars located just outside the edge of HI disk. This fraction, and hence the escape fraction, is progressively smaller in disks of smaller galaxies because their HI disks are thicker and more extended relative to the distribution of young stars compared to massive galaxies. Our results suggest that high-redshift galaxies are inefficient in releasing ionizing radiation produced by young stars into the intergalactic medium. We compare our predicted escape fraction of ionizing photons with previous results, and find a general agreement with both other simulation results and available direct detection measurements at $z \sim 3$. We also compare our simulations with a novel method to estimate the escape fraction in galaxies from the observed distribution of neutral hydrogen column densities along the lines of sights to long duration γ -ray bursts. Using this method we find escape fractions of the GRB host galaxies of 2–3%, consistent with our theoretical predictions.

Subject headings: cosmology: theory - galaxies: dwarf - galaxies: evolution - galaxies: formation - stars: formation - methods: numerical

1. INTRODUCTION

Star forming galaxies have a number of important effects on the surrounding intergalactic medium (IGM) and subsequent gas accretion. The ionizing radiation from galaxies is thought to be responsible for the re-ionization of the universe (e.g., Madau et al. 1999; Bolton et al. 2005), altering the thermal state of the IGM (Gnedin & Hui 1998; Gnedin 2000; Ricotti et al. 2000; Schaye et al. 2000; McDonald et al. 2001; Fechner & Reimers 2007), reducing gas accretion onto small dwarf galaxies (Efstathiou 1992; Thoul & Weinberg 1996; Dijkstra et al. 2004), and evaporating the existing gas in small halos (Barkana & Loeb 1999; Shaviv & Dekel 2003; Shapiro et al. 2004).

The amount of radiation emitted by galaxies into the IGM depends not only on the abundance of hot, young stars, but also on the spatial distribution of absorbing gas and dust in individual galaxies and their immediate surroundings. The escape of ionizing radiation from galaxies is therefore the focus of a number of observational and theoretical studies. Nevertheless, the “escape fraction”, f_{esc} , that characterizes the fraction of total ionizing radiation released into the IGM from individual galaxies remains poorly constrained.

Recent empirical measurements of the escape fraction from normal galaxies in the local universe (Leitherer et al. 1995; Heckman et al. 2001; Bergvall et al. 2006) and at high redshifts (Giallongo et al. 2002; Fernández-Soto et al. 2003;

Shapley et al. 2006)⁵ have generally produced modest values in the range of a few percent. In contrast, theoretical studies of the escape of ionizing radiation from high-redshift galaxies have largely been inconclusive. Many of the previous studies have applied simplified analytic models (Dove & Shull 1994; Haiman & Loeb 1997; Dove et al. 2000; Ricotti & Shull 2000; Wood & Loeb 2000; Clarke & Oey 2002; Fujita et al. 2003) that predicted a wide range of values for f_{esc} .

A more reliable estimate can be derived from self-consistent cosmological numerical simulations of galaxy formation that include three-dimensional radiative transfer and model the three-dimensional distribution of absorbing gas in and around individual galaxies. This approach is computationally challenging and has been attempted only recently at a range of redshifts, from $z \sim 20$ (Alvarez et al. 2006) to more modest redshifts $z \gtrsim 2$ (Razoumov & Sommer-Larsen 2006, 2007), where a comparison with the observations is possible.

In this paper, we continue this line of work using fully self-consistent cosmological simulations that include radiative transfer and resolve the interstellar medium in modest-sized galaxies at high redshifts. Our work is similar but complementary to the work of Razoumov & Sommer-Larsen (2006, 2007). In both approaches, self-consistent cosmological simulations of normal galaxies are used. However, while Razoumov & Sommer-Larsen (2006, 2007) use the Smooth Particle Hydrodynamics (SPH) for modeling galaxies with modest numbers of stellar particles (up to several thousand), we apply Adaptive Mesh Refinement (AMR) method in this study to reach a larger spatial dynamic range.

⁵ Note that both Giallongo et al. (2002) and Shapley et al. (2006) quote larger values, up to 15%. However, the quoted numbers are for *relative* escape fractions between the 1500 and the Lyman limit. The *absolute* escape fractions are actually about 3%, as we discuss in more detail in §6.

¹ Particle Astrophysics Center, Fermi National Accelerator Laboratory, Batavia, IL 60510, USA; gnedin@fnal.gov

² Kavli Institute for Cosmological Physics, The University of Chicago, Chicago, IL 60637, USA

³ Department of Astronomy & Astrophysics, The University of Chicago, Chicago, IL 60637 USA

⁴ Enrico Fermi Institute, The University of Chicago, Chicago, IL 60637, USA

Razoumov & Sommer-Larsen (2006, 2007) use the exact ray-tracing method for modeling the radiative transfer of ionizing radiation from simulated galaxies without taking into account effects of radiative transfer during simulation, while we use an approximate Optically Thin Variable Eddington Tensor (OTVET) method of Gnedin & Abel (2001) with radiative transfer calculations performed during the course of simulation self-consistently.

Most importantly, in this work we explicitly include absorption by dust, which allows a direct comparison with observational estimates of the escape fraction. Given the differences between Razoumov & Sommer-Larsen (2006, 2007) and our approaches, a comparison of the results is useful for estimating the range of systematic numerical uncertainties in the problem, where a rigorous convergence study is not yet feasible.

The paper is organized as follows. In § 2 we describe the simulations and numerical techniques used in our study. In § 3 we provide operational definition of the escape fraction and in § 4 we describe our model for dust absorption of the ionizing radiation. We present the results of the study in § 5 and discuss their implications in § 6.

2. SIMULATION

The simulation we use in this paper is described in detail by Tassis et al. (2006, where it is labeled as FNEQ-RT). Here we briefly summarize its setup and numerical parameters.

The simulation is performed using the Eulerian, gas dynamics + N -body Adaptive Refinement Tree (ART) code (Kravtsov et al. 1997, 2002). A large dynamic range is achieved through the use of Adaptive Mesh Refinement (AMR) in both the gas dynamics and gravity calculations. The calculation is started from a random realization of a Gaussian density field at $z = 50$ in a periodic box of $6h^{-1}$ Mpc in a flat Λ CDM model ($\Omega_m = 1 - \Omega_\Lambda = 0.3$, $\Omega_b = 0.043$, $h = 0.7$, $n_s = 1$, and $\sigma_8 = 0.9$). A Lagrangian region corresponding to five virial radii of a Milky Way sized galaxy at $z = 0$ is identified and evolved with 2.6×10^6 dark matter particles with masses of $9.2 \times 10^5 h^{-1} M_\odot$.

The code employs a uniform 64^3 grid to cover the entire computational box. The Lagrangian region is, however, always unconditionally refined to the third refinement level, corresponding to the effective grid size of 512^3 . As the matter distribution evolves, the code adaptively and recursively refines the mesh in high-density regions beyond the third level up to the maximum allowed 9th refinement level, which corresponds to the comoving spatial resolution of 260 pc, or physical resolution of 65(50) pc at $z = 3(4)$.

The ART code computes metallicity-dependent, non-equilibrium gas cooling “on the fly” based on the abundances of five atomic species and molecular hydrogen. Star formation and feedback (both radiative and thermal via supernova explosions and stellar winds) are included, as described in Tassis et al. (2006).

The self-consistent 3D radiative transfer of UV radiation from individual stellar particles is followed with the OTVET algorithm (Gnedin & Abel 2001). The details of our implementation of the OTVET algorithm on adaptively refined meshes will be described elsewhere (Gnedin & Kravtsov 2007, in preparation). A comparison of our radiative transfer scheme with several other existing numerical implementations for the time-dependent and spatially-inhomogeneous radiative transfer is presented in Iliev et al. (2006) and in the follow-up paper (Iliev et al. 2007, in preparation).

In addition to the main progenitor of the Milky Way type galaxy, the fully refined Lagrangian region contains several dozens of smaller galaxies spanning a wide range of masses. We will use all these systems to estimate the escape fraction of ionizing radiation from star forming regions for galaxies of different masses and star formation rate (SFR).

3. METHOD

Because our simulation includes an approximate treatment of the radiative transfer self-consistently, the non-equilibrium abundances of all ions for each cell in the AMR grid hierarchy are available throughout the calculation. We can thus measure the opacity at a given frequency along a given direction from any point in the simulation volume to any other point.

Since the opacity can only increase along a given line of sight, the escape fraction is, in general, a function of the distance from the source. We choose to measure this distance in units of the virial radius of a given galaxy and we measure the escape fraction at 0.5, 1, and 2 virial radii from the center of the galaxy (defined as the peak of the dark matter density). Unless specified otherwise, hereafter we use the escape fraction at one virial radius as our fiducial working definition of the escape fraction.

In computing the escape fraction, it is important to separate satellite galaxies from isolated ones. When a small satellite galaxy is located within a larger galaxy, the concept of virial radius and escape fraction becomes ambiguous. Therefore, we only consider isolated galaxies and only include sources that actually reside in (i.e. gravitationally bound to) the main galaxy, thus excluding the satellites. In computing the continuum absorption by ionic species we include the detailed velocity structure of the galactic and infalling gas, although we find that ignoring the gas velocity field makes no measurable difference on the escape fraction.

Operationally, the escape fraction f_{esc} of a specific galaxy at a given redshift is then a function of two variables: the frequency and the direction of propagation of escaping radiation:

$$f_{\text{esc}} \equiv f_{\text{esc}}(\nu, \vec{\theta}). \quad (1)$$

For studies of reionization of the universe and the Lyman-alpha forest, the most important quantity is the escape fraction of ionizing radiation,

$$f_{\text{esc}}^j(\vec{\theta}) \equiv \frac{\int d\nu f_{\text{esc}}(\nu, \vec{\theta}) \sigma_\nu^j S_\nu}{\int d\nu \sigma_\nu^j S_\nu}, \quad (2)$$

where σ_ν^j is the photo-ionization cross-section for the specie j ($j = \text{HI}, \text{HeI}, \text{HeII}$) and S_ν is the spectrum of the sources of radiation. In our simulation, we include only stellar sources and compute the ionizing radiation spectra using the Starburst99 package (Leitherer et al. 1999). We assume continuous star formation, 0.04 solar metallicity (typical of galaxies in our simulation), and a Salpeter initial mass function over a mass range from 1 to $100 M_\odot$. The spectral shape is shown in Figure 4 of Ricotti et al. (2002). Note that the Starburst99 spectral shape is computed for the unobscured stellar population, which is the appropriate spectral shape to use in equation (2), which explicitly includes the f_{esc} factor.

However, observationally the escape fraction of ionizing radiation is difficult to determine, since it requires measuring the whole ionizing spectrum. Instead, the escape fraction at the hydrogen ionization edge (Lyman limit), $f_{\text{esc}}(\nu_0)$, is usually measured in observational studies. We present the relationship between these two quantities in the appendix.

TABLE 1
PARAMETERS FOR THE DUST EXTINCTION LAW FITS

Term	Λ_i (μm)	a_i	b_i	p_i	q_i
SMC dust model					
1	0.042	185	90	2	2
2	0.08	27	15.5^a	4	4
3	0.22	0.005	-1.95	2	2
4	9.7	0.010	-1.95	2	2
5	18	0.012	-1.8	2	2
6	25	0.030	0	2	2
7	0.067	10	1.9	4	15
LMC dust model					
1	0.046	90	90	2	2
2	0.08	19	21	4.5	4.5
3	0.22	0.023	-1.95	2	2
4	9.7	0.005	-1.95	2	2
5	18	0.006	-1.8	2	2
6	25	0.02	0	2	2
7	0.067	10	1.9	4	15

^a Values changed from Pei (1992) are shown in bold.

4. ABSORPTION BY DUST

Incorporating dust absorption into the simulations for calculating the escape fraction is critical, because dust may contribute significantly to the absorption of ionizing radiation (e.g. Weingartner & Draine 2001). Unfortunately, properties of dust in high-redshift galaxies are not known well. In particular, dust absorption cross section depends on the dust composition and grain size distribution, which is measured only in nearby galaxies. In our analysis, we adopt the dust extinction curves for Large and Small Magellanic Clouds (LMC and SMC respectively) from Weingartner & Draine (2001) as representative of high redshift galaxies, because low metallicities of these galaxies are closer to typical metallicities of high-redshift galaxies in our simulation.

A convenient parameterization for the dust extinction law in LMC and SMC is given by Pei (1992), based on the earlier data,

$$\sigma_\nu^d = \sigma_0 \sum_{i=1}^7 f(\lambda/\lambda_i, a_i, b_i, p_i, q_i), \quad (3)$$

where the fitting function f has the form

$$f(x, a, b, p, q) = \frac{a}{x^p + x^{-q} + b}. \quad (4)$$

We correct the fits of Pei (1992) using the newer data from Weingartner & Draine (2001) by adding the seventh term in equation (3) in order to account for the narrow and asymmetric shape of the FUV peak in the dust extinction law. We also change values for some parameters from those adopted by Pei (1992). The values for the parameters we use are listed in Table 1, and we show in bold changes from Pei (1992).

The overall normalization for the dust cross section is determined by parameters $\sigma_{0,\text{LMC}} = 5.6 \times 10^{-22} \text{ cm}^2$ and $\sigma_{0,\text{SMC}} = 1.1 \times 10^{-22} \text{ cm}^2$. With these functional forms, the dust cross sections for both LMC and SMC fit the plotted curves of Weingartner & Draine (2001) to a few percent accuracy.

In order to limit the range of possible dust effects, we consider three extreme dust models: 1) a model with no dust at all, 2) a model in which we assume that the dust column density scales with neutral (atomic and molecular) gas column

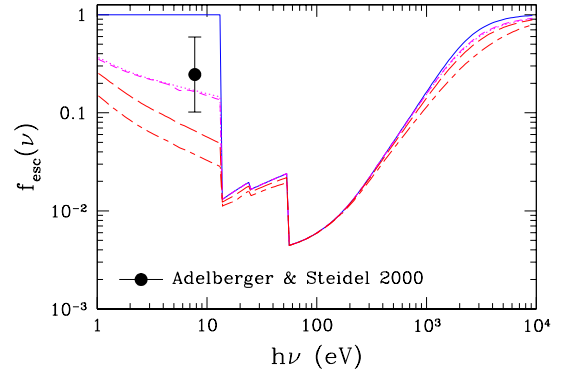


FIG. 1.— The frequency dependence of the angular averaged escape fraction for the central galaxy at $z = 3$ for several dust models: no dust (solid line), SMC dust with instant sublimation (eq. [5], dotted line), LMC dust with instant sublimation (eq. [5], short-dashed line), and SMC dust with no sublimation (eq. [6], long-dashed line). In addition, we also show with a short-long-dashed line the SMC no sublimation model with the dust cross section increased by a factor of 3, as a certain *overestimate* of the dust absorption. The black point with error-bars shows the extinction at 1600 from Adelberger & Steidel (2000, derived as $A_{1600} = 4.43 + 1.99\beta$ with $\beta = -1.46 \pm 0.48$).

density,

$$N_{\text{dust}} = \frac{Z}{Z_0} \times (N_{\text{H1}} + 2N_{\text{H}_2}) \quad (5)$$

(where Z is the gas metallicity), and 3) a model where the dust column density scales with the total gas column density (both neutral and ionized),

$$N_{\text{dust}} = \frac{Z}{Z_0} \times N_{\text{H}}, \quad (6)$$

where $Z_0 = 0.32$ (0.2) is the gas-phase metallicity of the LMC (or SMC, Welty et al. 1997, 1999). Note that emission line studies (Peimbert et al. 2000; Keller & Wood 2006) usually indicate somewhat larger values for both metallicities than the absorption line metallicities that we adopt. If we adopted larger values for the LMC and SMC metallicities, the dust effect on our measured escape fractions would be even *smaller*.

Physically, equation (5) implies a complete instant sublimation of dust in the ionized gas, while equation (6) implies no dust sublimation at all. Of course, the truth lies somewhere in between, but these two extreme cases bracket the range of possibilities.

Figure 1 shows the angular averaged escape fraction for the Milky Way progenitor galaxy at $z = 3$ as a function of frequency. We show several dust models, together with typical reddening correction for Lyman Break Galaxies from Adelberger & Steidel (2000). We also show the SMC no sublimation dust model with dust cross section arbitrarily increased by a factor of 3. As we have mentioned above, the no sublimation model is likely to overestimate the effect of dust absorption. Since it is highly unlikely that uncertainties in our adopted value for the SMC metallicity and the dust extinction curve are as large as a factor of 3, this latter model serves as an absolute (and, likely, implausibly high) upper limit for the dust absorption.

A rather unexpected feature of Figure 1 is that the escape fraction above the Lyman limit is almost independent of the dust absorption. In order to understand this phenomenon, we show in Figure 2 the distributions of escape fractions from all positions within the central galaxy in a fixed, randomly selected direction on the sky. The distributions have similar shapes: they are weak functions of f_{esc} for $0 < f_{\text{esc}} < 1$

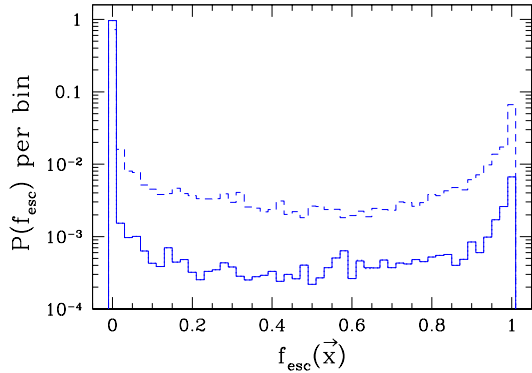


FIG. 2.— The luminosity weighted distribution of the escape fraction at the Lyman limit in a random direction on the sky from all positions within the central galaxy for the SMC instant sublimation dust model (our fiducial one). Three separate distributions are shown: absorption by gas only (dotted line), absorption by dust only (dashed line), and total absorption (dust + gas, solid line). Notice that the gas-only distribution is essentially identical to the total distribution, because $Z\sigma^d \ll \sigma^{\text{HI}}$ at the Lyman limit; so the dotted line coincides with the solid one. The histograms are normalized to add up to 1, so the spike at $f_{\text{esc}} \approx 0$ contains most of the data points.

and exhibit a primary peak at $f_{\text{esc}} \approx 0$ and a secondary peak at $f_{\text{esc}} \approx 1$. Thus, the escaping radiation is produced *not* by sources in a semi-opaque medium, with each source attenuated by a similar amount, but by a small fraction of essentially unobscured sources. We discuss this point in detail in § 5 below (see Fig. 8).

For a distribution like those in Figure 2, the effects of dust absorption can be easily understood, if we ignore the “translucent points” at $0 < f_{\text{esc}} < 1$ and use a toy-model distribution for the gas-only $f_{\text{esc,HI}}$,

$$p(f_{\text{esc,HI}}) = \alpha\delta(1 - f_{\text{esc,HI}}) + (1 - \alpha)\delta(f_{\text{esc,HI}}), \quad (7)$$

where $\alpha \ll 1$ is constant and $\delta(x)$ is a Dirac delta function. The average escape fraction in this model is simply

$$\langle f_{\text{esc,HI}} \rangle = \int_0^1 f_{\text{esc,HI}} P(f_{\text{esc,HI}}) df_{\text{esc,HI}} = \alpha. \quad (8)$$

If the dust absorption is included, then the escape fraction at each location is changed by a factor that depends on the dust opacity,

$$f_{\text{esc}} = f_{\text{esc,HI}} e^{-\tau_d} \equiv e^{-\tau_{\text{HI}} - \tau_d}.$$

At the locations where $f_{\text{esc,HI}} \approx 1$ ($\tau_{\text{HI}} \ll 1$), the effect of dust is negligible (since $\tau_d \ll \tau_{\text{HI}}$). At locations where $\tau_d \gtrsim 1$, the hydrogen opacity is already so large that no radiation escapes from this position, irrespective of how much dust is mixed with the gas. As the result, the escape fraction does not change at all.

In reality, “translucent points” with $0 < f_{\text{esc}} < 1$ are affected by dust, but their integrated contribution to the average escape fraction remains small. In the no sublimation dust model, the situation may be more complex, since there is dust absorption in the ionized gas. However, Figure 1 demonstrates that this is not a large effect.

At frequencies below the Lyman limit the distribution of f_{esc} from dust is similar to Figure 2, but there is no gas absorption. Because dust absorption is weaker than gas absorption, the average escape fraction at these frequencies is much larger and increases to unity as the frequency decreases down to infra-red.

The important result of this section is that, while dust absorption is the dominant effect for UV radiation below the

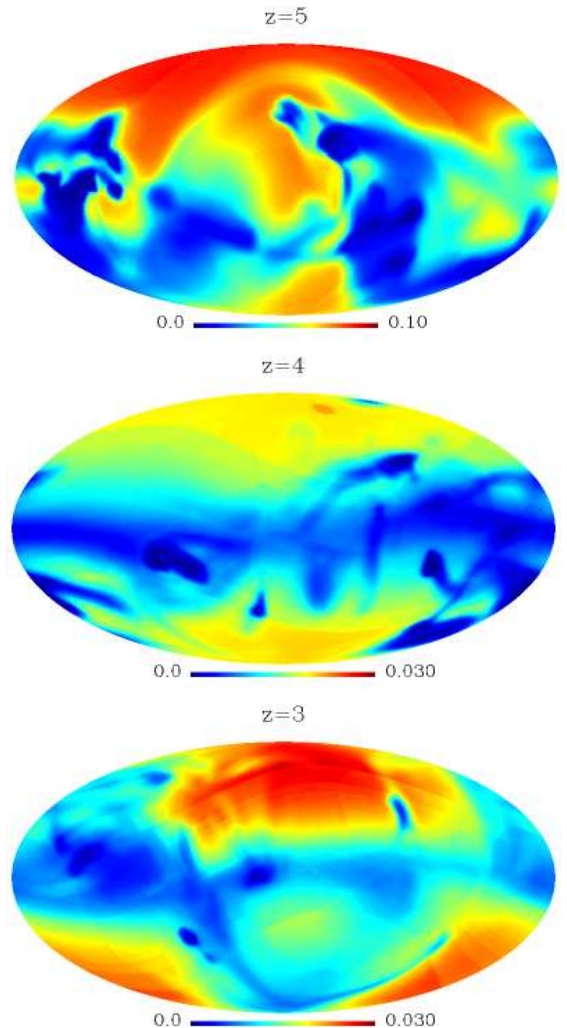


FIG. 3.— The escape fraction of HI ionizing radiation $f_{\text{esc}}^{\text{HI}}$ as a function of direction, as visible from the center of the Milky Way type galaxy, at the virial radius of the galaxy at $z = 5, 4,$ and 3 . The sky is oriented in coordinates aligned with galactic gas disk such that the disk is horizontal in the middle of the plot. Note a different color scale for $z = 5$ image.

Lyman Limit, it does not substantially affect the escape fraction of ionizing radiation in our model galaxies, as Figure 1 demonstrates.

In the rest of this paper, we adopt the SMC instant sublimation model as our fiducial dust model, but we note that our final results are not sensitive to this particular choice.

5. RESULTS

Figure 3 shows the escape fraction of hydrogen ionizing radiation $f_{\text{esc}}^{\text{HI}}$ (eq. 2) as seen from the center of the central galaxy (the Milky Way progenitor) at three different redshifts. The celestial coordinates in Figure 3 are aligned with the principal axes of the galaxy (“galactic” coordinates), with the plane of the disk of the galaxy crossing the middle of the plot. Typically, the escape fraction is close to zero along the plane of the disk and approaches maximum values near the poles, although there are significant small-scale variations at all redshifts that underscore the complex, perturbed nature of high redshift disk galaxies. At $z = 5$ the galaxy is experiencing a substantial major merger (and a lesser one at $z = 3$), so the angular distribution of escape fractions is more irregular at these epochs.

Another interesting feature of the f_{esc} distribution shown

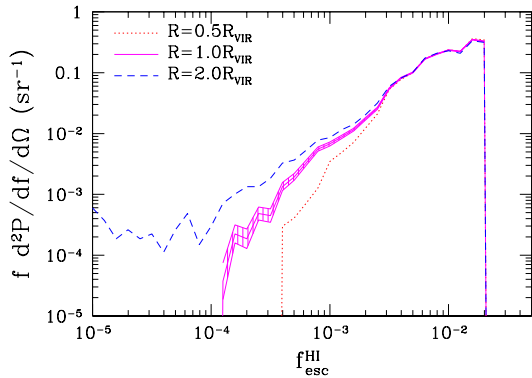


FIG. 4.— The probability per unit log and per unit solid angle for having a specific value of the escape fraction of HI ionizing radiation for the central galaxy at $z=4$ for 3 distances from the galaxy center (as measured in units of the galaxy virial radius). The shaded region around the middle curve shows the Poisson errors due to the finite number of pixels in the angular maps.

in Figure 3 is a few small very opaque (dark blue) clouds of gas that block ionizing radiation at larger distances. These clouds can be counterparts of the Lyman Limit absorbers observed in the spectra of distant quasars. Previous studies, based on lower resolution simulations, have indicated that Lyman Limit systems tend to cluster around large galaxies (Kohler & Gnedin 2007). Our simulations confirm that such clouds do exist around high-redshift galaxies.

We have checked that, as we integrate further in distance, more of Lyman Limit systems fall inside the radius of integration, and the “sky”, as seen from the center of the galaxy, appears progressively more opaque. The sky should become completely opaque at a distance of a few mean free paths for ionizing radiation. At $z=4$ the mean free path for ionizing radiation is about $85 h^{-1}$ co-moving Mpc (Miralda-Escudé 2003), much larger than the size of our computational box. Thus, we cannot actually reach the full opacity with our current simulation. However, the important point to make is that the mean free path is much larger than a virial radius of any galaxy at these redshifts, so the concept of the “escape fraction” is well defined and robust at intermediate redshifts.

Figure 4 illustrates this point in a quantitative way. It shows the probability density for having a specific value of the escape fraction on a celestial sphere at different distances from the center of the main progenitor of the Milky Way-sized galaxy. As the distance from the galaxy increases, the tail of the distribution at low escape fractions grows, as Lyman limit systems cover a progressively larger fraction of the sky. However, at distance comparable to the virial radius of the galaxy the effect of Lyman limit systems is small, as can be seen from the plot: the fraction of the sky below $f_{\text{esc}}^{\text{HI}} = 0.003$ increases from 3% to only 6% as the distance increases from $0.5R_{\text{VIR}}$ to $2R_{\text{VIR}}$.

Poisson errors on the probability density shown in Figure 4 remain small for escape fractions well below 10^{-3} , indicating that angular maps from Figure 3 resolve the structure in the gas down to that level. Of course, the small-scale structure in the gas is limited by the finite resolution of our simulation.

Figure 5 presents the main result of this paper: the angular averaged escape fraction for hydrogen ionizing radiation as a function of galaxy mass or star formation rate at a range of redshifts. We only show results for the galaxies which are resolved down to the maximum ninth level of refinement. This resolution criterion corresponds approximately to a minimum mass of $10^{10} M_{\odot}$ (or $\gtrsim 10^4$ dark matter particles). A gen-

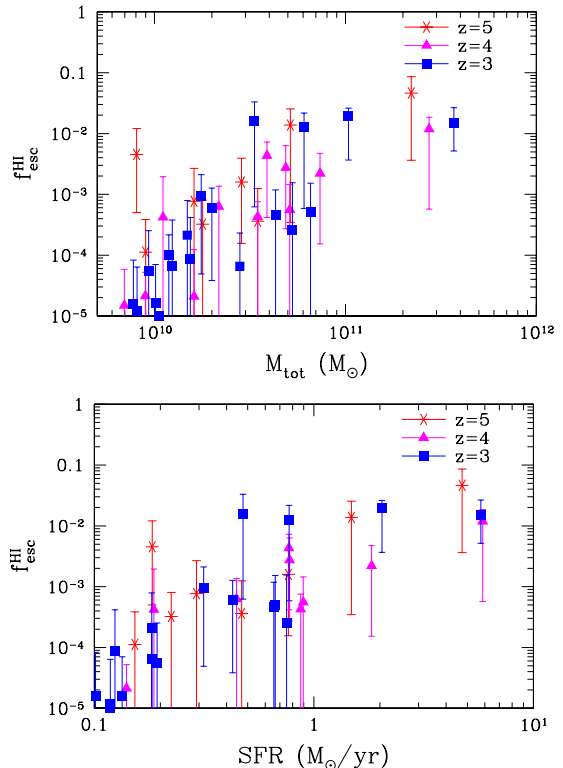


FIG. 5.— The angular averaged escape fraction of HI ionizing radiation as a function of galaxy mass (top) and star formation rate (bottom) at three redshifts (squares). The error-bars show the 10%–90% range for all possible directions.

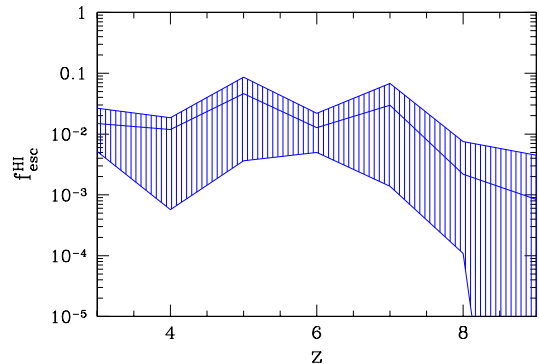


FIG. 6.— The evolution of the angular averaged escape fraction of HI ionizing radiation for the most galaxy ($M_{\text{tot}} = 4 \times 10^{11} M_{\odot}$ at $z=3$). The shaded band shows the 10%–90% range for all possible directions.

eral trend of increasing escape fraction with increasing galaxy mass and SFR is clearly observed: the escape fraction changes by approximately two orders of magnitude from $\approx 10^{-4}$ to $\approx 0.02-0.05$ for total masses between 10^{10} to $4 \times 10^{11} M_{\odot}$ (or SFR from 0.1 to $\approx 7 M_{\odot} \text{ yr}^{-1}$). At the same time, the figure also shows that there is little change with redshift, from $z=5$ to $z=3$, either in the values of the escape fraction or in the dominant trend with mass or SFR.

Figure 6 further illustrates the lack of redshift evolution in the escape fraction found in our simulations. The figure shows the average escape fraction of the most massive Milky Way progenitor in the simulation at different redshifts, along with the variation in escape fraction in different directions. While the escape fraction fluctuates with redshift, a spread in the escape fraction in different directions at a given redshift is

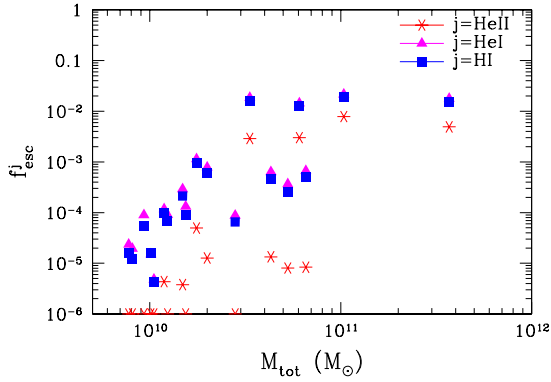


FIG. 7.— The mass dependence of the escape fraction of ionized radiation for three ionic species at $z = 3$ (similar to the top panel of Figure 5). We show only well-resolved galaxies and omit error-bars for clarity. The escape fractions are clumped at the level of 10^{-6} to allow all points to be visible on the graph.

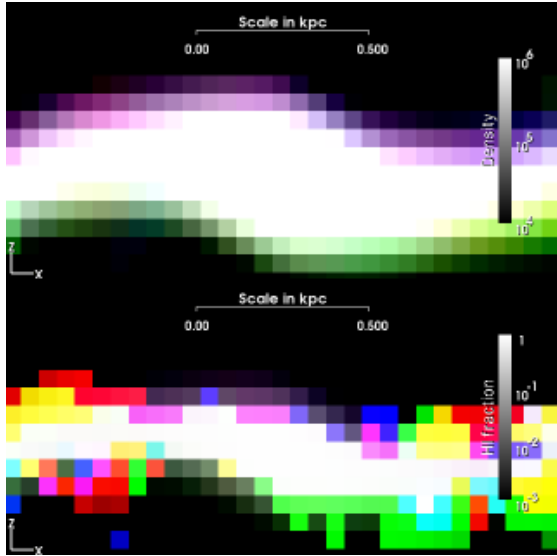


FIG. 8.— The pseudo-color composite edge-on view of the main galaxy. The top half shows the gas density, while the bottom half depicts the neutral hydrogen fraction. Each image is composed of 3 snapshots from the simulation taken 10 Myr apart at $z \sim 4$ and combined as red, green, and blue channels of a color image. The predominance of purple (red and blue) color on top and green color on bottom indicates that the galactic disk oscillates globally on a time scale of about 20 Myr. The oscillation pattern is much more chaotic in HI image outside of about 1 kpc. (This figure should be viewed in color.)

much larger than the variation in the average escape fraction with redshifts at $z < 7$. A similarly weak trend is found by most well resolved galaxies from our simulation.

There is clearly a significant drop in the escape fraction at HeII ionization threshold. This is further illustrated in Figure 7, which shows all three escape fractions for ionizing radiation as a function of the total mass for model galaxies. We note that HI and HeI are invariably close to each other, while HeII escape fractions are systematically much lower. This behavior is again completely expected, as only active galactic nuclei are thought to fully (i.e. doubly) ionize helium.

We also study the mechanism for the escape of ionizing radiation from galactic disks in our simulations and for the predicted small values of f_{esc} . As Figure 2 demonstrates, the ionizing radiation that escapes is emitted preferentially by unobscured sources, with only a small fraction of all sources being unobscured at any given time (rather than being emitted

by the majority of sources, which are only partially obscured). In order to visualize the regions of a galaxy where these unobscured sources reside, Figure 8 shows a pseudo-color composite image of three different snapshots from the simulation closely spaced in time.

The edge-on disk of the main galaxy is shown in the total gas density (top) and in the HI fraction (bottom). Three snapshots 10 Myr apart at $z \sim 4$ are overlaid together so that the first snapshot is shown in red, the second in green, and the last one in blue. If the gas distribution did not change between the snapshots, then the image would appear as an equal combination of red, green, and blue, i.e. as a pure grayscale. In reality, however, the upper surface of the disk appears purple (red plus blue), while the bottom surface is pure green. This means that the galactic disk oscillates with a period of about 20 Myr: the disk bended downwards between the first (red) snapshot and the second (green) snapshot, but returned to the first configuration in the third (blue) snapshot, so that the first and third snapshots look almost identical, blending into a single purple color. Oscillating modes with shorter wavelengths are also visible in the image.

This behavior is clearly visible in the total gas density image and in the HI fraction image within the inner 0.5–0.7 kpc; the HI disk oscillates much more violently at larger radii. This is not surprising, because the oscillations of the HI edge are subject to the positive feedback. As the HI edge oscillates and uncovers ionizing sources, the ionizing intensity in a given point is likely to increase (similarly to how the ionizing intensity increases when isolated HII regions merge during reionization).

Figure 8 thus shows why ionizing radiation of some young stars can leave the galaxy with virtually no attenuation. The cold HI disk, where young stars form is very thin (~ 100 – 200 pc). Some of the stars may have sufficient velocity to move outside the edge of the HI disk while they are still young, bright emitters of UV photons. For example, a star traveling at 10 km s^{-1} will move by $\approx 100 \text{ pc}$ in 10^7 years. In addition, the outer edge of the HI disk is changing significantly on the same time scale. These changes can expose some of the young stars and clear the way for the ionizing radiation to leave the system. *The escaped ionizing radiation is thus mostly due to a small fraction of stars in a thin shell surrounding the HI disk.*

The relative constancy of the escape fraction with redshift or SFR that we find is then a simple consequence of the galactic disks oscillating by a comparable amount on 10 Myr time scale. Note that this time scale is close to the local dynamical time scale of the dense high-redshift disks and lifetime of massive, UV-bright stars. Such oscillations are thus likely dynamical in origin: the disk can be perturbed by mergers and interactions with satellites, which are only weakly correlated with SFR or redshift (unless a disk goes into a starburst phase).

This picture also explains why the escape fraction decreases steeply for lower mass galaxies. Gas distribution in dwarf galaxies is relatively more extended in comparison to the stellar distribution in our simulations, due to lower efficiency of star formation in dwarfs relative to massive galaxies (see Tassis et al. 2006, for detailed discussion). Stars are thus concentrated towards central regions of the disk and a smaller fraction of them can reach the edge of HI disk or get exposed by fluctuations of its boundary. Note, however, that resolution of dwarf galaxies in our simulations is considerably worse than for the massive galaxies. This explanation and the trend

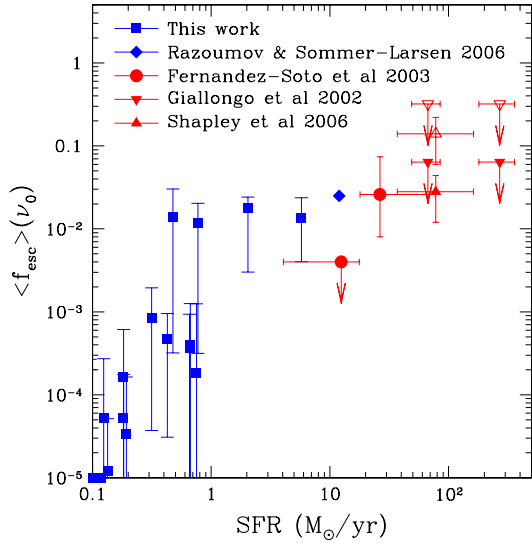


FIG. 9.— A comparison of the angular averaged escape fraction at hydrogen ionization edge at $z = 3$ from various determinations. Filled red/gray upward triangle and circles show the observational measurements from Shapley et al. (2006) and Fernández-Soto et al. (2003) respectively, presented as average values for their data samples. Two filled red/gray downward triangles show the upper limits from Giallongo et al. (2002). Both Shapley et al. (2006) are Giallongo et al. (2002) points are corrected from the measured relative escape fraction to the absolute escape fraction, as explained in the text (open symbols show the original uncorrected measurements). The filled blue/black diamond is the simulation results of Razoumov & Sommer-Larsen (2006) for the single galaxy they report the star formation rate for. Filled blue/black squares with error-bars show our results, similar to Figure 5.

with mass will thus need to be verified in the future by higher resolution simulations.

6. DISCUSSION AND CONCLUSIONS

To summarize the current understanding of the escape fraction of photons at the ionizing threshold of hydrogen, we show in Figure 9 both simulation predictions and observational constraints available at $z = 3$. The simulation predictions are taken from Razoumov & Sommer-Larsen (2006) and our work. Observational constraints are from Giallongo et al. (2002, upper limits only), Fernández-Soto et al. (2003), and Shapley et al. (2006). The measurements of Giallongo et al. (2002) are for individual galaxies with SFR taken from Pettini et al. (1998). The measurement of Shapley et al. (2006) is an average of 14 star-forming galaxies at $z \sim 3$. The SFR is estimated based on the observed UV flux and corrected for dust extinction for $\langle E(B-V) \rangle = 0.11$. Both Giallongo et al. (2002) and Shapley et al. (2006) measurements are corrected from the relative measurements of the ratio $f_{\text{esc}}(912)/f_{\text{esc}}(1500)$ they report to the absolute measurement of $f_{\text{esc}}(912)$ by adopting a value of $f_{\text{esc}}(1500) = 0.2$ from Adelberger & Steidel (2000). This correction factor is also consistent with other observed estimates of reddening at 1500 (Pettini et al. 1998; Steidel et al. 2001; Shapley et al. 2006). The measurements of Fernández-Soto et al. (2003) are averaged over 14(13) high(low) luminosity galaxies found at $1.9 < z < 3.5$ in the Hubble Deep Field (the second one is actually an upper limit). The star formation rates are conversions of the observed UV flux using the scaling relation from Madau et al. (1998), and are corrected for dust extinction assuming $E(B-V) = 0.1$ and the extinction law from Calzetti et al. (2000). Fernández-Soto et al. (2003) measure the absolute escape fraction, so no correction is applied to their points.

There still exists a gap between simulations and observa-

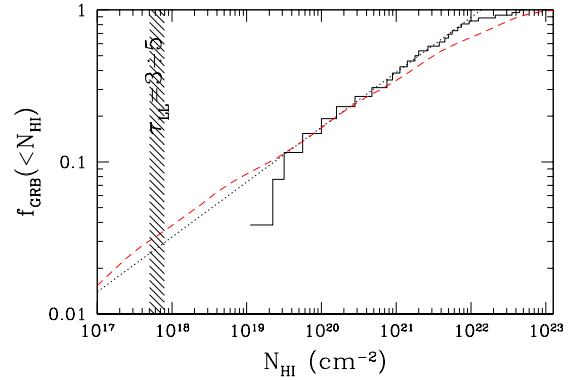


FIG. 10.— A comparison of the cumulative distribution of HI column densities toward ionizing sources from our simulation at $z = 3$ (dashed line) with that measured in the host galaxies of long duration γ -ray bursts at $z > 2$. The black solid line shows the observational data compiled by Vreeswijk et al. (2004) and Jakobsson et al. (2006), as well as the data for two additional sources from Shin et al. (2006) and Ruiz-Velasco et al. (2007). In two cases (GRB 060124 and GRB 060607) only upper limits have been measured. The dotted line is a power-law fit to the observational data for the range of HI column densities between $10^{19.5} \text{ cm}^{-2}$ and $10^{21.5} \text{ cm}^{-2}$.

tions in the luminosity and SFR parameter space. While our simulations model modest-mass galaxies, observational measurements are reported mostly for the brightest, $\gtrsim L_*$ galaxies. Nevertheless, the simulations are tantalizingly close to reaching a similar range of luminosity and SFR covered by the observations. Both the observations and our simulations indicate little (if any) trend in the *absolute* escape fraction with the galaxy mass or star formation rate, except for a rapid drop in f_{esc} for smaller mass galaxies. Our simulations indicate that this characteristic scale corresponds to about $\text{SFR} \sim 1 M_{\odot} \text{ yr}^{-1}$ or $M_{\text{tot}} \sim 10^{11} M_{\odot}$, although an upper limit of $f_{\text{esc}} < 0.4\%$ from Fernández-Soto et al. (2003) at $\text{SFR} \sim 10 M_{\odot} \text{ yr}^{-1}$ may indicate that simulations overestimate escape fractions in galaxies with $\text{SFR} \lesssim 10 M_{\odot} \text{ yr}^{-1}$. The level of the disagreement (if any) cannot yet be accurately deduced from our simulations, and, formally, the Fernández-Soto et al. (2003) upper limit is fully consistent with our results. Note also that Siana et al. (2007) in their recent study of the Lyman continuum escape fractions in galaxies at $z \sim 1$ also find small values ($f_{\text{esc}} \lesssim 0.1$), which is consistent with weak evolution of escape fractions we find in our simulations. The general agreement between our results and observations is definitely encouraging and may indicate that relative distribution of the young stars and UV absorbing gas is modeled faithfully in our high-resolution AMR simulations.

An interesting alternative way of constraining the escape fraction observationally, independent of the observed UV light, is offered by the observed distribution of HI column densities in the host galaxies of long duration γ -ray bursts (GRBs; Chen, Prochaska, & Gnedin 2007, in preparation). Assuming that GRBs sample the distribution of young stars in an unbiased fashion, the fraction of young stars located in ionized regions with small or negligible attenuation of UV radiation should correspond to the fraction of GRBs with HI column densities lower than some threshold value corresponding to the transition between neutral and ionized hydrogen.

Figure 10 shows the observed distribution of HI column densities in spectra of GRBs with confirmed redshifts of $z > 2$, compared to the corresponding distribution in our simulation at $z = 3$. The observed distribution is remarkably close to a power-law for $10^{19.5} \text{ cm}^{-2} < N_{\text{HI}} < 10^{21.5} \text{ cm}^{-2}$. Extrapolating this power-law to lower column densities of $\approx (5-8) \times$

10^{17} cm^2 (or $\tau_{LL} = 3-5$, appropriate for the boundary between the ionized and neutral gas⁶) implies that about 2–3% of all GRBs are located in ionized regions in which the UV radiation of their progenitors should have escaped freely into the IGM, so that

$$f_{\text{esc}} \approx f_{\text{GRB}}(N_{\text{HI}} < (5-8) \times 10^{17} \text{ cm}^2) = 0.02-0.03.$$

This value is remarkably close to the escape fractions of $\approx 1-3\%$ measured in our simulations. This test also provides strong support for our interpretation of why the escape fractions are so low.

Note that the HI column density distribution toward ionizing sources (i.e. column densities from source locations to one virial radius, as explained in §3) from our fiducial simulation at $z = 3$ is reasonably close to the observed distribution of N_{HI} from GRBs for $N_{\text{HI}} < 3 \times 10^{21} \text{ cm}^2$. At higher column density we do not expect a good agreement between our simulation and the data, because the simulation does not incorporate the physics of formation and self-shielding of molecular hydrogen correctly, which becomes important in that regime. Thus, the simulation is expected to overpredict N_{HI} column densities, because in reality some of this HI is in molecular form.

While higher resolution simulations and deeper observations are needed to bridge the remaining small gap in the probed star formation regime between the data and the theory, our results suggest that average escape fractions from bright galaxies at intermediate redshifts do not depend strongly on galaxy properties or redshift. This is interesting because this implies that porosity of the interstellar medium in galaxies, and hence its opacity to ionizing radiation, does not dramatically change at higher star formation rates, as expected in

⁶ The specific location of the ionization edge of a galaxy depends on a number of factors and does not correspond to a particular value of τ_{LL} . A value of $\tau_{LL} = 1$, which corresponds to the suppression of ionizing background by only a factor of 3, is certainly not enough to make the gas substantially neutral. A value of $\tau_{LL} = 10$ is, on the other hand, enough to make

some of the theoretical models (e.g., Clarke & Oey 2002). Note that observed escape fractions at higher star formation rates are consistent with being simply an extrapolation of the trend seen in simulations at lower rates. If this is indeed the case, this implies absence of a well-defined critical SFR above which the escape fraction sharply increases to unity.

At the same time, the low values of escape fractions found in our simulations suggest that high-redshift galaxies are quite inefficient in emitting ionizing radiation produced by their young stars into the intergalactic medium, with escape fractions decreasing sharply for galaxies of $M_{\text{tot}} \lesssim 10^{11} M_{\odot}$ (or $\text{SFR} \lesssim 1 M_{\odot} \text{ yr}^{-1}$). This conclusion potentially has important implications for the contribution from normal galaxies to the early reionization of the universe and for the relative role of galaxies and quasars in keeping the universe ionized at intermediate redshifts.

We thank Douglas Rudd for constructive and useful comments on the draft of this paper. This work was supported in part by the DOE and the NASA grant NAG 5-10842 at Fermilab, by the NSF grants AST-0206216, AST-0239759, and AST-0507596, and by the Kavli Institute for Cosmological Physics at the University of Chicago. Supercomputer simulations were run on the IBM P690 array at the National Center for Supercomputing Applications and San Diego Supercomputing Center (under grant AST-020018N) and the Sanssouci computing cluster at the Astrophysikalisches Institut Potsdam. This work made extensive use of the NASA Astrophysics Data System, arxiv.org preprint server, and the HEALPix⁷ (Górski et al. 2005) package.

the gas even at the mean cosmic density largely neutral. Thus, a value of τ_{LL} around 3 to 5 should correspond to the approximate location for the galaxy ionization edge.

⁷ <http://healpix.jpl.nasa.gov>

APPENDIX

ESCAPE FRACTION FOR IONIZING RADIATION AND THE ESCAPE FRACTION AT THE IONIZATION EDGE

In order to facilitate comparison between the theoretical and observational results, in Figure 11 we show a relationship between the theoretically relevant escape fraction of ionizing radiation (i.e. an integral quantity, as defined in eq. 2, since it determines the ionization state of the IGM) and the escape fraction at the hydrogen ionization edge (Lyman limit), which is usually measured in observational studies. We find a tight correlation between the two quantities in the form

$$f_{\text{esc}}^{\text{HI}} = 1.25 f_{\text{esc}}(\nu_0), \quad (\text{A1})$$

which is helpful for relating observationally measured and theoretically relevant quantities. We use this relation in Fig. 9 when comparing observational and theoretical values on the same plot.

REFERENCES

- Adelberger, K. L. & Steidel, C. C. 2000, *ApJ*, 544, 218
 Alvarez, M. A., Bromm, V., & Shapiro, P. R. 2006, *ApJ*, 639, 621
 Barkana, R. & Loeb, A. 1999, *ApJ*, 523, 54
 Bergvall, N., Zackrisson, E., Andersson, B.-G., Arnberg, D., Masegosa, J., & Östlin, G. 2006, *A&A*, 448, 513
 Bolton, J. S., Haehnelt, M. G., Viel, M., & Springel, V. 2005, *MNRAS*, 357, 1178
 Calzetti, D., Armus, L., Bohlin, R. C., Kinney, A. L., Koornneef, J., & Storchi-Bergmann, T. 2000, *ApJ*, 533, 682
 Clarke, C. & Oey, M. S. 2002, *MNRAS*, 337, 1299
 Dijkstra, M., Haiman, Z., Rees, M. J., & Weinberg, D. H. 2004, *ApJ*, 601, 666
 Dove, J. B. & Shull, J. M. 1994, *ApJ*, 430, 222
 Dove, J. B., Shull, J. M., & Ferrara, A. 2000, *ApJ*, 531, 846
 Efsthathiou, G. 1992, *MNRAS*, 256, 43P
 Fechner, C. & Reimers, D. 2007, *A&A*, 463, 69
 Fernández-Soto, A., Lanzetta, K. M., & Chen, H.-W. 2003, *MNRAS*, 342, 1215
 Fujita, A., Martin, C. L., Mac Low, M.-M., & Abel, T. 2003, *ApJ*, 599, 50
 Giallongo, E., Cristiani, S., D’Odorico, S., & Fontana, A. 2002, *ApJ*, 568, L9
 Gnedin, N. Y. 2000, *ApJ*, 542, 535
 Gnedin, N. Y. & Abel, T. 2001, *New Astronomy*, 6, 437
 Gnedin, N. Y. & Hui, L. 1998, *MNRAS*, 296, 44
 Górski, K. M., Hivon, E., Banday, A. J., Wandelt, B. D., Hansen, F. K., Reinecke, M., & Bartelmann, M. 2005, *ApJ*, 622, 759
 Haiman, Z. & Loeb, A. 1997, *ApJ*, 483, 21
 Heckman, T. M., Sembach, K. R., Meurer, G. R., Leitherer, C., Calzetti, D., & Martin, C. L. 2001, *ApJ*, 558, 56
 Iliiev, I. T., et al. 2006, *MNRAS*, 371, 1057
 Jakobsson, P., et al. 2006, *A&A*, 460, L13

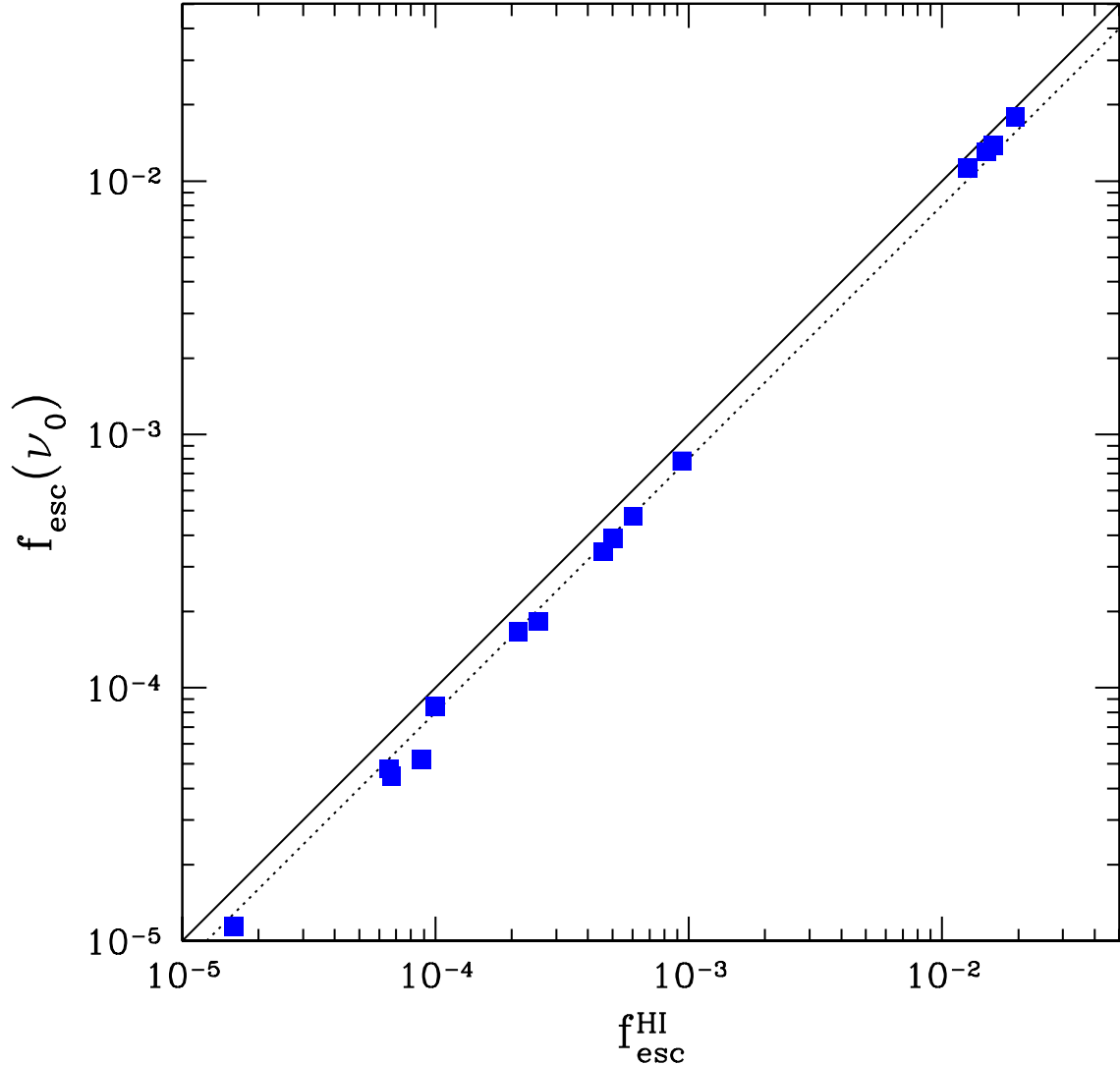


FIG. 11.— A comparison of the angular averaged escape fraction for HI ionizing radiation (eq. 2) with the angular averaged escape fraction at the ionization edge (Lyman limit, the quantity usually measured in observational work), $h\nu_0 = 13.6\text{ eV}$. Solid and dotted lines show the $f_{\text{esc}}^{\text{HI}} = f_{\text{esc}}(\nu_0)$ and $f_{\text{esc}}^{\text{HI}} = 1.25f_{\text{esc}}(\nu_0)$ relations respectively.

- Keller, S. C. & Wood, P. R. 2006, *ApJ*, 642, 834
 Kohler, K. & Gnedin, N. Y. 2007, *ApJ*, 655, 685
 Kravtsov, A. V., Klypin, A., & Hoffman, Y. 2002, *ApJ*, 571, 563
 Kravtsov, A. V., Klypin, A. A., & Khokhlov, A. M. 1997, *ApJS*, 111, 73
 Leitherer, C., Ferguson, H. C., Heckman, T. M., & Lowenthal, J. D. 1995, *ApJ*, 454, L19+
 Leitherer, C., et al. 1999, *ApJS*, 123, 3
 Madau, P., Haardt, F., & Rees, M. J. 1999, *ApJ*, 514, 648
 Madau, P., Pozzetti, L., & Dickinson, M. 1998, *ApJ*, 498, 106
 McDonald, P., Miralda-Escudé, J., Rauch, M., Sargent, W. L. W., Barlow, T. A., & Cen, R. 2001, *ApJ*, 562, 52
 Miralda-Escudé, J. 2003, *ApJ*, 597, 66
 Pei, Y. C. 1992, *ApJ*, 395, 130
 Peimbert, M., Peimbert, A., & Ruiz, M. T. 2000, *ApJ*, 541, 688
 Pettini, M., Kellogg, M., Steidel, C. C., Dickinson, M., Adelberger, K. L., & Giavalisco, M. 1998, *ApJ*, 508, 539
 Razoumov, A. O. & Sommer-Larsen, J. 2006, *ApJ*, 651, L89
 Razoumov, A. O. & Sommer-Larsen, J. 2007, *ArXiv Astrophysics e-prints*
 Ricotti, M., Gnedin, N. Y., & Shull, J. M. 2000, *ApJ*, 534, 41
 Ricotti, M., Gnedin, N. Y., & Shull, J. M. 2002, *ApJ*, 575, 33
 Ricotti, M. & Shull, J. M. 2000, *ApJ*, 542, 548
 Ruiz-Velasco, A. E., et al. 2007, *ArXiv e-prints*, 706
 Schaye, J., Theuns, T., Rauch, M., Efstathiou, G., & Sargent, W. L. W. 2000, *MNRAS*, 318, 817
 Shapiro, P. R., Iliev, I. T., & Raga, A. C. 2004, *MNRAS*, 348, 753
 Shapley, A. E., Steidel, C. C., Pettini, M., Adelberger, K. L., & Erb, D. K. 2006, *ApJ*, 651, 688
 Shaviv, N. J. & Dekel, A. 2003, *astro-ph/0305527*
 Shin, M.-S., et al. 2006, *ArXiv Astrophysics e-prints*
 Siana, B., et al. 2007, *ApJ in press (astro-ph/0706.4093)*, 706
 Steidel, C. C., Pettini, M., & Adelberger, K. L. 2001, *ApJ*, 546, 665
 Tassis, K., Kravtsov, A. V., & Gnedin, N. Y. 2006, *ApJsubmitted (astro-ph/0609763)*
 Thoul, A. A. & Weinberg, D. H. 1996, *ApJ*, 465, 608
 Vreeswijk, P. M., et al. 2004, *A&A*, 419, 927
 Weingartner, J. C. & Draine, B. T. 2001, *ApJ*, 548, 296
 Welty, D. E., Frisch, P. C., Sonneborn, G., & York, D. G. 1999, *ApJ*, 512, 636
 Welty, D. E., Lauroesch, J. T., Blades, J. C., Hobbs, L. M., & York, D. G. 1997, *ApJ*, 489, 672
 Wood, K. & Loeb, A. 2000, *ApJ*, 545, 86